7. Howard, J. C., Cardinaux, F. & Scheraga, H. A. Block copolymers of amino acids. II. Physicochemical data on copolymers containing L-alanine or L-phenylalanine. *Biopolymers* **16,** 2029–2051 (1977).
8. Gratzer, W. B. & Doty, P. A conformational examination of poly-L-alanine and poly-D,L-alanine in aqueous solution. *J. Am. Chem. Soc.* **85,** 1193–1197 (1963).
9. Inoue, K. *et al*. Preparation and conformation of hexaarmed star poly(β-benzyl-L-aspartates) utilizing hexakis(4-aminophenoxy) cyclotriphosphazene. *J. Am. Chem. Soc.* **116,** 10783–10784 (1994).
10. Kubota, S. & Fasman, G. D. The β conformation of polypeptides of valine, isoleucine, and threonine in solution and solid-state: optical and infrared studies. *Biopolymers* **14,** 605–631 (1975).
11. Kricheldorf, H. R. *α-Aminoacid-N-Carboxyanhydrides and Related Materials* (Springer, New York, 1987).
12. Kricheldorf, H. R. in *Models of Biopolymers by Ring-Opening Polymerization* (ed. Penczek, S.) (CRC, Boca Raton, 1990).
13. Idelson, M. & Blout, E. R. Polypeptides XV. Infrared spectroscopy and the kinetics of the synthesis of polypeptides: primary amine initiated reactions. *J. Am. Chem. Soc.* **79,** 3948–3957 (1957).
14. Idelson, M. & Blout, E. R. Polypeptides XVIII. A kinetic study of the polymerization of amino acid *N*-carboxyanhydrides initiated by strong bases. *J. Am. Chem. Soc.* **80,** 2387–2393 (1958).
15. Lundberg, R. D. & Doty, P. Polypeptides XVII. A study of the kinetics of the primary amine-initiated polymerization of *N*-carboxyanydrides with special reference to configurational and stereochemical effects. *J. Am. Chem. Soc.* **79,** 3961–3972 (1957).
16. Deming, T. J. Polypeptide materials: new synthetic methods and applications. *Adv. Mater.* **9,** 299–311 (1997).
17. Deming, T. J. Transition metal–amine initators for preparation of well-defined poly(γ-benzyl-L-glutamate). *J. Am. Chem. Soc.* **119,** 2759–2760 (1997).
18. Fetters, L. J. in *Encyclopedia of Polymer Science and Engineering* 2nd edn 19–25 (Wiley-Interscience, New York, 1987).
19. Webster, O. Living polymerization methods. *Science* **251,** 887–893 (1991).
20. Collman, J. P., Hegedus, L. S., Norton, J. R. & Finke, R. G. *Principles and Applications of Organotransition Metal Chemistry* 2nd edn (University Science, Mill Valley, 1987).
21. Uhlig, E., Fehske, G. & Nestler, B. Z. Reaktionen cyclischer Carbonsaueureanhydride mit (α,α′-Dipyridyl)-(cyclooctadien-1,5)-nickel. *Anorg. Allg. Chem.* **465,** 141–146 (1980).
22. Sano, K., Yamamoto, T. & Yamamoto, A. Preparation of Ni- or Pt-containing cyclic esters by oxidative addition of cyclic carboxylic anhydrides and their properties. *Bull. Chem. Soc. Jpn* **57,** 2741–2747 (1984).
23. Castaño, A. M. & Echavarren, A. M. Reactivity of a nickelacycle derived from aspartic acid: alkylations, insertions, and oxidations. *Organometalics* **13,** 2262–2268 (1994).
24. Block, H. *Poly(γ-benzyl-L-glutamate) and Other Glutamic Acid Containing Polymers* (Gordon and Breach, New York, 1983).
25. Noshay, A. & McGrath, J. E. *Block Copolymers* (Academic, New York, 1977).

Correspondence and requests for materials should be addressed to T.J.D. (e-mail: tdeming@engineering.ucsb.edu).

Interrelated influence of iron, light and cell size on marine phytoplankton growth

William G. Sunda & Susan A. Huntsman

National Marine Fisheries Service, 101 Pivers Island Road, Beaufort, North Carolina 28516, USA

The sub-optimal growth of phytoplankton and the resulting persistence of unutilized plant nutrients (nitrate and phosphate) in the surface waters of certain ocean regions has been a long-standing puzzle[1,2]. Of these regions, the Southern Ocean seems to play the greatest role in the global carbon cycle[3,4], but controversy exists as to the dominant controls on net algal production. Limitation by iron deficiency[4,5], light availability[1,6,7] and grazing by zooplankton[2] have been proposed. Here we present the results from culture experiments showing that the amount of cellular iron needed to support growth is higher under lower light intensities, owing to a greater requirement for photosynthetic iron-based redox proteins by low-light acclimatized algae. Moreover, algal iron uptake varies with cell surface area, such that the growth of small cells is favoured under iron limitation, as predicted theoretically[8]. Phytoplankton growth can therefore be simultaneously limited by the availability of both iron and light. Such a co-limitation may be experienced by phytoplankton in iron-poor regions in which the surface mixed layer extends below the euphotic zone—as often occurs in the Southern Ocean[6,7]—or near the bottom of the euphotic zone in more stratified waters. By favouring the growth of smaller cells, iron/light co-limitation should increase grazing by microzooplankton, and thus minimize the loss of fixed carbon and nitrogen from surface waters in settling particles[9,10].

We examined the iron uptake and growth dynamics of coastal diatoms (*Thalassiosira pseudonana* and *T. weissflogii*) and dinoflagellates (*Prorocentrum minimum* and *P. micans*) representing a range of cell diameters (3.5 to 30–32 μm) (Fig. 1). Experiments were run at light intensities of 500 and 50 μeinstein m^{-2} s^{-1} for *T. pseudonana* and *P. minimum* and at the higher intensity only for the other two species. The cells were grown at 20 °C on a 14 : 10 h light : dark cycle in EDTA-metal ion buffered media[11]. We measured the steady-state cellular Fe, Fe uptake rates, chlorophyll *a*, cell size

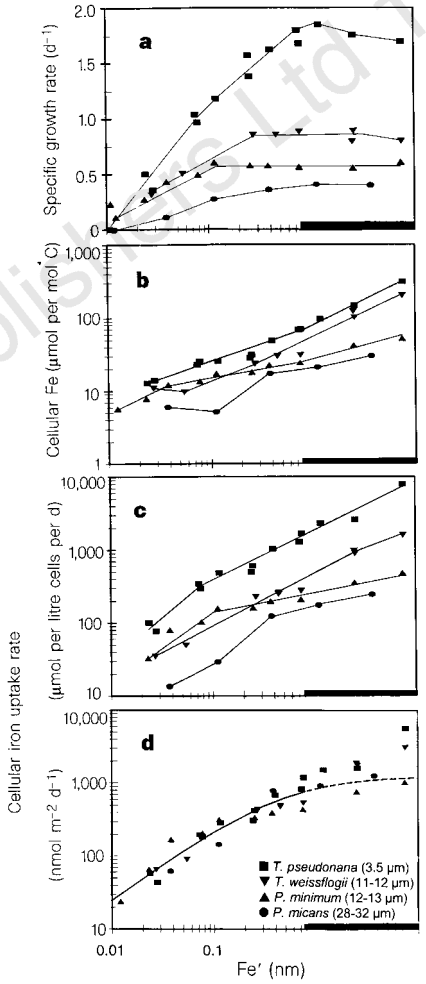

Figure 1 Relationships among specific growth rate, intracellular Fe : C (measured with radiotracers), Fe uptake rate (normalized to cell volume and equivalent spherical surface area), and [Fe′] for coastal eukaryotes of varying mean diameters grown at 500 μE m^{-2} s^{-1} (here μE indicates microeinstein). The 36‰ salinity media was enriched with EDTA/trace metal ion buffers and 32 μM $NaNO_3$, 2 μM Na_2HPO_4, 40 μM Na_2SiO_3, 10 nM Na_2SeO_3, 0.074 nM vitamin B_{12}, 0.4 nM biotin and 60 nM thiamin. Solid bar on the *x*-axis represents the region where Fe hydroxides are observed to precipitate[11]. Horizontal dimensions in all cases are proportional to total Fe. [Fe′] is the mean value over a 14 : 10 light : dark cycle and equals total dissolved Fe times 0.0025, 0.00166 and 0.00132 at light intensities of 500, 160 and 50 μE m^{-2} s^{-1}. The solid curve in **d** gives the modelled saturation curve as fitted to equation (1) by nonlinear regression ($R^2 = 0.90$) using data for [Fe′] ≤ 0.75 nM. Results presented here are mostly new, but also include some published[11] high-light data for *T. pseudonana*, *T. weissflogii* and *P. minimum*. The data include three separate experiments with *T. pseudonana*, and two each with *T. weissflogii* and *P. minimum*. A single *T. pseudonana* experiment with four Fe levels run in triplicate yielded mean standard deviations of ±3.2, 3.9, 8.5, 8.4 and 10% for specific growth rate, Fe : C, Fe per litre cell volume, and C- and volume-normalized uptake rates, respectively. Experimental procedures and analyses are as described previously[11].

and specific growth rates over a range of concentration of dissolved inorganic Fe species ([Fe′])[11], the primary parameter that controls Fe uptake in eukaryotic marine algae[8,12,13]. Studies of growth rate only were made at low light with *P. micans* and at three light intensities with the coastal cyanobacterium *Synechococcus bacillaris*.

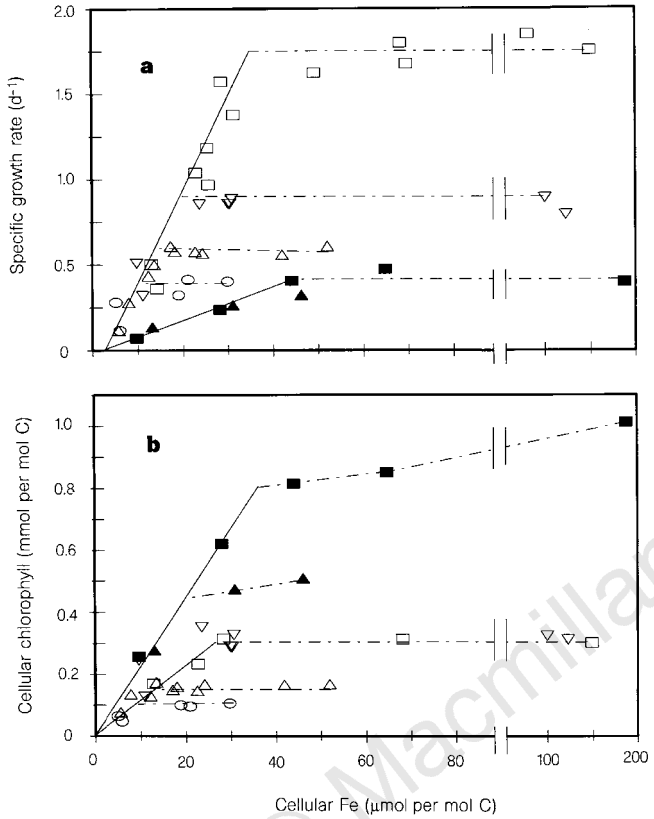

Figure 2 Specific growth rate (**a**) and Chl *a* : C (**b**) as functions of intracellular Fe : C at high (500 μE m^{-2} s^{-1}; open symbols) and low light (50, closed symbols). Light was controlled by neutral density screens. Cellular parameters were measured as described previously[11]. Symbol shapes are as defined in Fig. 1d.

At high light, Fe limitation of growth rate in all four eukaryotic species occurred at or below the measured solubility limit for [Fe′] with respect to Fe hydroxide precipitation[11] (Fig. 1a), above which [Fe′] should be constant. Growth rate was inversely related to cell size under both Fe-sufficient and Fe-limiting conditions.

Cellular Fe normalized to carbon (Fig. 1b) and to cell volume (data not shown) increased with Fe concentration and decreased with cell size. The steady-state uptake rate for Fe, calculated by multiplying cell Fe by specific growth rate, showed an even steeper positive dependence on external Fe and inverse dependence on cell size due to the decrease in growth rate with increasing cell size and with decreasing [Fe′] (Fig. 1c). But when normalized to cell surface area, uptake rate (V_{SA}) in all four species fitted a single saturation equation for nutrient uptake (Fig. 1d):

$$V_{SA} = V_{max}[Fe']/([Fe'] + K_s) \quad (1)$$

where $V_{max} = 1{,}276\ \text{nmol m}^{-2}\ \text{d}^{-1}$ and $K_s = 0.51$ nM. Thus, the larger cells had low volume- or C-normalized uptake rates because of low surface-to-volume ratios. The similarity in surface-normalized uptake rates is predicted from previous findings which show that Fe uptake in coastal and oceanic species occurs at theoretically limiting rates determined by the kinetics of Fe transfer to surface uptake sites and available space on the cell's membrane[8,11].

Iron uptake by diatoms continues to increase with total Fe in the region of hydroxide precipitation (Fig. 1d), implying that Fe in the hydroxides is available for uptake[11]. But the availability of Fe hydroxides is much less than that of Fe′ because the ratio of hydroxides to [Fe′] where the additional uptake occurs is ~10,000.

Under Fe-limitation, specific growth rate (μ) was linearly related to cell Fe : C ratio for all four species (Fig. 2a), consistent with the role of Fe as a catalyst in biosynthesis[14]. Linear regression of the high-light data gave the relationship

$$\mu = B([\text{Fe:C}] - m) \quad (R^2 = 0.91) \quad (2)$$

where m (3 mmol mol^{-1}) is the Fe : C ratio needed for cell maintenance at zero growth rate. The slope, $B = 49{,}360$ mol C (mol Fe)$^{-1}$ d^{-1}, defines the iron use efficiency (IUE) for a photoperiod of 14 h d^{-1}, which translates to 84,600 (49,360 × 24/14) for continuous light. The latter value compares favourably with the IUE (72,000 mol C (mol Fe)$^{-1}$ d^{-1}) computed from cell models of the Fe needed to support photosynthesis, respiration and nitrate assimilation,

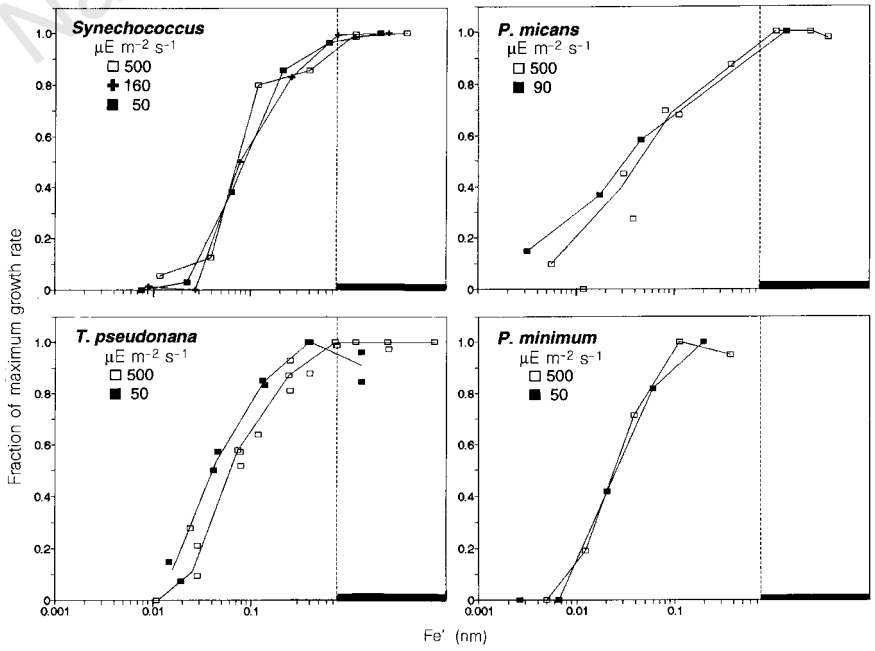

Figure 3 Plot of μ/μ_{max} against [Fe′] at growth-saturating and growth-limiting light intensities. The vertical dotted line marks the solubility limit for [Fe′].

assuming 1 : 1 : 1 : 1 stoichiometry for photosystem II : cytochrome b_6/f complex : cytochrome c : photosystem I and that flavodoxin replaces ferredoxin[14]. At high Fe : C, growth rates reached maximum values, which were inversely related to cell size (Fig. 2a).

At one tenth of the previous light intensity, the Fe-limited growth rate of *T. pseudonana* and *P. minimum* also fitted equation (2), but the slope of the relationship between μ and [Fe : C] was reduced fivefold to 9,700 mol C (mol Fe^{-1}) d^{-1} (Fig. 2a). Maximum growth rates were also reduced, but by lower amounts (1.9- to 3.8-fold). The higher Fe : C needed to support growth at low light occurs because of reduced light capture and electron flow per photosynthetic unit (PSU). Cells acclimatize to low light largely by increasing the number of PSUs[15,16], which include light harvesting pigments, photo-reaction centres and electron transfer molecules. PSUs contain many cytochromes and Fe/S proteins, and account for much of the cell's ion content[14,15]. Thus, a low-light adaptive increase in PSUs involves a large increase in cell Fe.

The chlorophyll *a* : C ratio of Fe-limited cells was proportional to Fe : C. The Chl : Fe ratio determined from the slope of the plots of cell Chl *a* against Fe (Fig. 2b) was higher at low light (21.3 mol Chl (mol Fe)$^{-1}$) than at high light (11.5) owing to photoacclimatization. From IUE models[14,15], 50% of the cell's Fe should occur within PSUs at high light and 90% at low light. By dividing cell Chl *a* : Fe by the fraction of Fe in PSUs, and multiplying this value by 24 Fe atoms per PSU[14], we calculate that there are 550 Chl *a* molecules per PSU at high light and 570 at low light, similar to values (500–1,300) observed in coastal eukaryotic species at similar light intensities[16]. Our results indicate an approximate stoichiometry for Fe and Chl within PSUs as predicted by Raven[15]. The results imply that the well-known decrease in Chl under Fe-limitation results from a decrease in PSUs due to insufficient Fe for synthesis of needed cytochromes and Fe/S proteins.

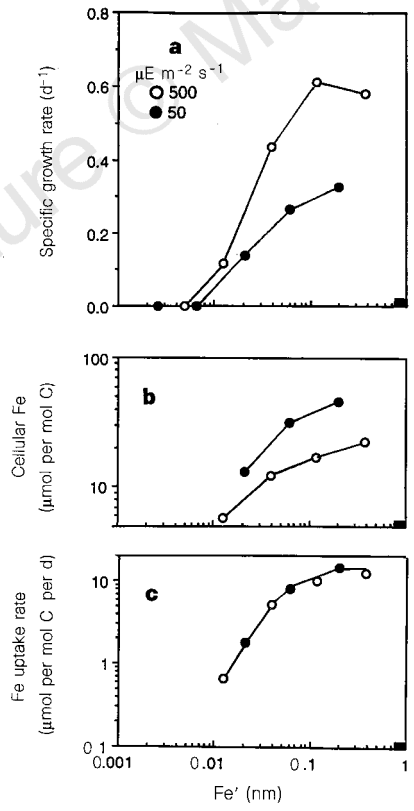

Figure 4 Relationships among specific growth rate, intracellular Fe : C, Fe uptake rate, and [Fe′] for *P. minimum* at growth-saturating and limiting light (500 and 50 μE m^{-2} s^{-1}).

As cells need higher Fe : C for growth under low light, we had expected low-light acclimatized cells to require higher external Fe levels to achieve maximum growth rate (μ_{max}). Despite this expectation, plots of μ/μ_{max} against [Fe′] for the four species tested show similar results irrespective of light intensity (Fig. 3). The reasons for this surprising result can be seen from relationships among specific growth rate, cell Fe : C and C-normalized Fe uptake rate for *P. minimum* (Fig. 4). As light is decreased, μ decreases because of light limitation (Fig. 4a). Because the cells are taking up Fe at the maximum rates permitted by physics and chemistry (see above), the uptake rate at low light for a given [Fe′] cannot exceed that at high light, and indeed relationships between uptake rate and [Fe′] are independent of light intensity (Fig. 4c). The decrease in growth rate with light limitation causes cell Fe : C to increase (Fig. 4b) because of the inverse relationship between Fe : C and μ at constant steady-state uptake rate, V_{ss}

$$\text{Cell Fe:C} = V_{ss}/\mu \qquad (3)$$

This increase allows the cells to synthesize additional PSUs needed for low light acclimization.

Unlike other potentially growth-limiting nutrients (N, P, Si and Zn) which are highly soluble and can reach high concentrations, levels of biologically available Fe′ in sea water are limited by the solubility of Fe hydroxide. Once these hydroxides form, additional Fe inputs will not increase [Fe′], only Fe hydroxides, which are much less available than soluble Fe′ (ref. 13) and also will aggregate and settle out from sea water[17]. Although most of the dissolved Fe is chelated by organic ligands[18–20], the chelated Fe should not be directly available for algal uptake[8,12] and will not affect the solubility limit on [Fe′]. We argue that the low solubility of Fe′ places a limit on the amount of metabolic Fe a cell can accumulate for a given size and, thus, on the maximum growth rate it can achieve under various light conditions. Such a limit would be most important in coastal and estuarine systems which receive high Fe inputs from continental sources[17]. This idea is supported by our finding that the minimum [Fe′] needed to achieve maximum growth rate just equals the [Fe′] solubility limit in three out of our five coastal species under both saturating and growth-limiting light. In no case does it exceed this limit. We argue that this occurs because over the past ~2 billion years, the maximum [Fe′], and, thus, the maximum growth rate that cells could achieve, were fixed by this limit.

Our results indicate that Fe and light limitation and cell size are all integrally linked. In the open ocean, Fe levels are much lower than in coastal waters and [Fe′] should generally be below the solubility limit[19–22]. Iron limits algal growth in at least some oceanic systems[5,23,24] and cells are more likely to be Fe-limited under low irradiance. Adaptation to low light at the bottom of the euphotic zone in stratified regions will lead to high cell Fe : C ratios and, therefore, high removal of Fe relative to other nutrients (C, N and P). This higher removal should drive these systems towards greater Fe limitation, and may largely explain the observed depletion of Fe within deep Chl maxima[21,22]. The combined Fe/light limitation will favour the growth of small cells, consistent with the observed dominance of small prokaryotes and the paucity of larger eukaryotes in deep Chl maxima[25,26].

Martin *et al.*[4,5] have argued that the limited draw-down of nitrate and CO_2 in the Southern Ocean results from Fe limitation of algal growth, whereas Nelson, Mitchell and others[6,7] argue that it results primarily from light limitation due to deep mixed layers and low overall solar irradiance. We argue that they are both correct, and that the phytoplankton are simultaneously limited by Fe and light. Furthermore, by favouring the growth of small cells, Fe/light co-limitation should increase grazing rates by microzooplankton and reduce settling rates of algal cells and faecal pellets, and thereby increase nutrient cycling and decrease export of carbon and nutrients from surface waters[9,10]. □

Received 15 April; accepted 3 October 1997.

1. Hart, T. J. On the phytoplankton in the southwest Atlantic and Bellinghausen Sea, 1929–31. *Discovery Rep.* **8,** 1–268 (1934).
2. Cullen, J. T. Hypotheses to explain high nutrient conditions in the open sea. *Limnol. Oceanogr.* **36,** 1579–1599 (1991).
3. Sarmiento, J. L. & Toggweiler, J. R. A new model for the role of the oceans in determining atmospheric carbon dioxide levels. *Nature* **308,** 621–624 (1984).
4. Martin, J. H. Glacial–interglacial CO_2 change: The iron hypothesis. *Palaeooceanography* **5,** 1–13 (1990).
5. Martin, J. H., Fitzwater, S. E. & Gordon, R. M. Iron deficiency limits phytoplankton growth in Antarctic waters. *Global Biogeochem. Cycles* **4,** 5–12 (1990).
6. Nelson, D. M. & Smith, W. O. Sverdrup revisited: Critical depths, maximum chlorophyll levels, and the control of Southern Ocean productivity by the irradiance-mixing regime. *Limnol. Oceanogr.* **36,** 1650–1661 (1991).
7. Mitchell, B. G., Brody, E. A., Holm-Hansen, O., McCain, C. & Bishop, J. Light limitation of phytoplankton biomass and macronutrient utilization in the Southern Ocean. *Limnol. Oceanogr.* **36,** 1662–1677 (1991).
8. Hudson, R. J. M. & Morel, F. M. M. Iron transport in marine phytoplankton: kinetics of medium and cellular coordination reactions. *Limnol. Oceanogr.* **35,** 1002–1020 (1990).
9. Miller, C. B. *et al.* Ecological dynamics in the subarctic Pacific, a possibly iron-limited ecosystem. *Limnol. Oceanogr.* **36,** 1600–1615 (1991).
10. Price, N. M., Ahner, B. A. & Morel, F. M. M. The equatorial Pacific Ocean: Grazer controlled phytoplankton populations in an iron-limited ecosystem. *Limnol. Oceanogr.* **39,** 520–534 (1994).
11. Sunda, W. G. & Huntsman, S. A. Iron uptake and growth limitation in oceanic and coastal phytoplankton. *Mar. Chem.* **50,** 189–206 (1995).
12. Anderson, M. A. & Morel, F. M. M. The influence of aqueous iron chemistry on the uptake of iron by the coastal diatom *Thalassiosira weissflogii*. *Limnol. Oceanogr.* **27,** 789–813 (1982).
13. Rich, H. W. & Morel, F. M. M. The availability of well-defined iron colloids to the marine diatom *Thalassiosira weissflogii*. *Limnol. Oceanogr.* **35,** 652–662 (1990).
14. Raven, J. A. The iron and molybdenum use efficiencies of plant growth with different energy, carbon and nitrogen sources. *New Phytol.* **109,** 279–287 (1988).
15. Raven, J. A. Predictions of Mn and Fe use efficiencies of phototrophic growth as a function of light availability for growth and C assimilation pathway. *New Phytol.* **116,** 1–18 (1990).
16. Falkowski, P. G., Owens, T. G., Ley, A. C. & Mauzerall, D. C. Effects of growth irradiance levels on the ratio of reaction centers in two species of marine phytoplankton. *Plant Physiol.* **68,** 969–973 (1981).
17. Boyle, E. A., Edmond, J. M. & Sholkovitz, E. R. The mechanism of iron removal in estuaries. *Geochim. Cosmochim. Acta* **41,** 1313–1324 (1977).
18. Gledhill, M. & van den Berg, C. M. G. Determination of complexation of iron (III) with natural organic complexing ligands in seawater using cathodic stripping voltametry. *Mar. Chem.* **47,** 41–54 (1994).
19. Wu, J. & Luther, G. W. Complexation of Fe(III) by natural organic ligands in the Northwest Atlantic Ocean determined by a competitive equilibration method and kinetic approach. *Mar. Chem.* **50,** 159–177 (1995).
20. Rue, E. L. & Bruland, K. W. Complexation of iron(III) by natural organic ligands in the Central North Pacific as determined by a new competitive ligand equilibration/adsorptive cathodic stripping voltametric method. *Mar. Chem.* **50,** 117–138 (1995).
21. Martin, J. H. & Gordon, R. M. Northeast Pacific iron distributions in relation to phytoplankton productivity. *Deep-Sea Res.* **35,** 177–196 (1988).
22. Bruland, K. W., Orians, K. J. & Cowen, J. P. Reactive trace metals in the stratified central North Pacific. *Geochim. Cosmochim. Acta* **58,** 3171–3182 (1994).
23. Coale, K. H. *et al.* A massive phytoplankton bloom induced by an ecosystem-scale iron fertilization experiment in the equatorial Pacific Ocean. *Nature* **383,** 495–501 (1996).
24. Behrenfeld, M. J., Bale, A. J., Kolber, Z. S., Aiken, J. & Falkowski, P. G. Confirmation of iron limitation of phytoplankton photosynthesis in the equatorial Pacific. *Nature* **383,** 508–511 (1996).
25. Shimada, A., Hasegawa, T., Umeda, Kadoya, N. & Maruyama. Spatial mesoscale patterns of West Pacific picoplankton as analyzed by flow cytometry: their contribution to subsurface chlorophyll maxima. *Mar. Biol.* **115,** 209–215 (1993).
26. Takahashi, M. & Hori, T. The abundance of picoplankton in the subsurface chlorophyll maximum layer in subtropical and tropical waters. *Mar. Biol.* **79,** 177–186 (1984).

Acknowledgements. This paper was supported by grants from the Office of Naval Research.

Correspondence should be addressed to W.G.S. (e-mail: b.sunda@hatteras.bea.nmfs.gov).

Anisotropic upper-mantle stratigraphy and architecture of the Slave craton

M. G. Bostock

Department of Earth and Ocean Sciences, University of British Columbia, Vancouver, British Columbia, Canada V6T 1Z4

The Earth's physical properties show a dominantly radial structure which is the result of compositional differentiation, isochemical phase changes[1] and rheological layering[2]. Rheological layering is perhaps the most difficult to investigate using conventional seismological techniques because the seismic manifestation of this property, elastic anisotropy, may closely mimic the effects of isotropic heterogeneity[3]. Nonetheless, an improved characterization of Earth's rheological structure promises important insights into such processes as plate dynamics and continental evolution. Here, I present a methodology for effectively characterizing sharp transitions in anisotropic, upper-mantle structure using the coda of teleseismic P-waves. Application to seismograms from the Slave craton reveals a well-developed stratigraphy, at least in part anisotropic, with major boundaries occurring at nominal depths of 75, 135 and 195 km. The geometry and sharpness of these discontinuities suggest a structural origin, perhaps involving shallow subduction.

The Slave province is a small (2.1×10^5 km^2) Archaean craton located in Canada's Northwest Territories (Fig. 1), hosting the oldest dated rocks on Earth[4]. These rocks together with recent diamond discoveries in the region[5] have prompted considerable research interest in the Slave province with the objective of better understanding craton structure and evolution. A remote means of accessing the subcrustal, cratonic lithosphere involves the analysis of seismic energy arriving in the coda of teleseismic P. I have compiled a set of 907 broadband three-component seismograms recorded at five stations (YKW1–4, and RSNT) near Yellowknife, Northwest Territories, representing a total of 427 earthquakes. These events are well distributed in azimuth and epicentral distance (Fig. 1). Each seismogram contains the combined effects of Earth structure and earthquake source; the latter must be removed for the present purpose. Seismograms are source-normalized using an approach similar to conventional receiver function analysis[6], but incorporating a number of important modifications to improve resolution of subtle features in the seismic wavefield. These include a more effective P, S decomposition through inversion of the free surface transfer-matrix[7], and simultaneous deconvolution of multiple seismograms to isolate structural effects[8].

The product of this signal processing is essentially the S-wave contribution at early times to the Earth's impulse response. One may choose to associate this empirical Green's function with either one-dimensional or three-dimensional structure depending on the selection of seismograms used in simultaneous deconvolution. An effective means of presenting and analysing the impulse response is in colour-coded images of amplitude as a functions of time and epicentral distance, as has been used, for example, to characterize the Earth's long-period response[9]. The radial component impulse response for Yellowknife is shown in Fig. 2a from 5 s before to 30 s after arrival of direct P over the epicentral distance range from 30° to 100°. This image comprises a 514-seismogram subset of the

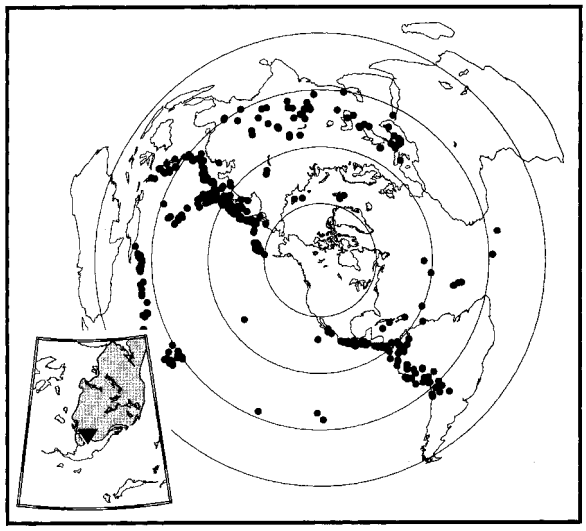

Figure 1 Azimuthal projection of the distribution of events (small black circles) recorded at Yellowknife and used in this study. Inset shows location of Yellowknife stations (triangle) relative to outline of Slave craton in grey. Circles represent 30° increments in distance from Yellowknife.